



Batch and fixed-bed column adsorption of crystal violet and safranin by zero-valent iron (nZVI) and nZVI-modified *S. cerevisiae*

Ulker Asli Guler*, Ozge Kundakci

Department of Environmental Engineering, Engineering Faculty, Cumhuriyet University, Sivas 58140, Turkey, email: ulkerasli@gmail.com (U.A. Guler), melusina4848@gmail.com (O. Kundakci)

Received 3 October 2017; Accepted 19 February 2018

ABSTRACT

Batch and continuous studies were conducted to examine the adsorption and degradation of zero-valent iron (nZVI) and nZVI-modified *S. cerevisiae* (magnetic yeast) to remove crystal violet (CV) and safranin (SF) from synthetic wastewater. The nZVI and magnetic yeast were characterized using FTIR, SEM, EDX, and BET analysis. pH, initial dye concentration, contact time, adsorbent dosage, temperature, ion selectivity, and the effect of ionic and cationic strength were examined. The adsorption equilibrium data are an excellent fit to the Langmuir, Freundlich, and Dubinin-Radushkevich (D-R) isotherm models. Different adsorption kinetics were used to examine the removal process of CV and SF, which followed a pseudo-second-order model. Adsorption was spontaneous. The adsorption of CV and SF dyes by nZVI-alginate and magnetic biosorbent-alginate in a column was studied. Regeneration efficiency was 76–87% after two cycles.

Keywords: nZVI; Magnetic yeast; Dye; Fixed-bed column; Regeneration

1. Introduction

Industrial effluents containing dye and toxic substances are considered a major source of contamination because dye residues are toxic, nondegradable, and have carcinogenic effects in the environment [1,2]. Crystal violet (CV) and safranin (SF) are cationic dyes. CV is generally used for coloring cloth and in the production of paints and printing inks [3,4]. SF is used to color sweets and cookies, in the leather and paper industries, and in research on histology, textile, cytology, and bacteriology [5].

Methods for removing dye from aqueous solution mainly consist of conventional technologies such as biological treatments [6], coagulation/flocculation [7], advanced oxidation processes [8], electroflotation [9], electrokinetic coagulation [10], and sorption [11]. Of all these methods, adsorption is one of the main means of treating dye effluents.

Recently, there has been growing interest in the application of nanoscale zero-valent iron (nZVI) as adsorbent for dye removal due to availability, rapid reaction kinetics, and low cost [12–14]. However, there are still some limitations

of nZVI technology in contaminant sequestration such as agglomeration, secondary iron pollution, oxidation by non-target compounds, and separation and recovery problems after using nZVI particles [15,16]. To address these problems, nZVI has been modified with materials such as pumice [12], diatomite [15], Tween-20 [17], kaolinite [18], bentonite [19], and microbial cells [20–23]. The present study reports on batch and column experiments intended to remove pollutants from water using nZVI and magnetic yeast. This material not only possesses the magnetic character of nZVI, but also has the good biosorption capability of yeast. To the best of our knowledge such magnetically modified cells have not been used for the removal of CV and SF dyes. According to the results, magnetic yeast is suitable for the use as adsorbent for the removal of CV and SF in wastewater. Generally, removal studies in literature are performed in batch systems. In order to understand availability in real industrial wastewater treatment, in this study laboratory-scale column studies were conducted.

The main objective of this study is to investigate the effectiveness of magnetic removal (adsorption and reduction) of CV and SF by nZVI and nZVI-modified *S. cerevisiae* (magnetic yeast) in batch and column systems. Magnetic

*Corresponding author.

yeast has a complex chemical and biological characterization, which makes it very interesting theoretically. First, nZVI and nZVI-modified *S. cerevisiae* cells were synthesized. Experimental data were examined at different operating conditions such as solution pH, contact time, initial dye concentration, temperature, ion selectivity, and ionic (0.1–1 M NaCl) and cationic strength (0.1–1 M Cu²⁺). Removal mechanisms were assessed with FTIR, SEM, and EDX analyses. Kinetic models and thermodynamics parameters were also investigated. Finally, regeneration and stability of the nZVI-alginate and magnetic yeast-alginate hydrogel beads were determined.

2. Materials and methods

2.1. Production of nZVI and magnetic yeast

The nZVI and magnetic yeast were synthesized with reduction of FeCl₂·4H₂O by NaBH₄ [24,25]. *S. cerevisiae* yeast used as a support material. 0.02 M FeCl₂·4H₂O solution (30 mL) and yeast (1.5 g) was placed into Erlenmeyer and then was stirred for 1 h with an ultrasonic shaker. Subsequently, 1 M NaBH₄ (100 mL) was added slowly into the solution. The synthesized materials were separated via vacuum filtration and it was washed few times with ethanol. After washing, the synthesized material was dried at 50°C for a period of 12 h and powdered to be used in adsorption experiments. The preparation of magnetic yeast composites had yeast to nZVI mass ratio of 1:1. The nZVI composites were obtained following the same process. The nZVI and magnetic yeast were stored in brown, sealed bottles for later use.

2.2. Production of nZVI-alginate and magnetic yeast-alginate hydrogel beads

The nZVI-alginate and magnetic yeast-alginate hydrogel beads were prepared via mixing the nZVI and magnetic yeast with 3 wt% alginate solution. Then small droplets into a 20 wt% CaCl₂ solution using a syringe were distributed. The preparation of nZVI-alginate and magnetic yeast-alginate hydrogel beads had analginate to adsorbent mass ratio of 3:1.

2.3. Batch studies

Effects of pH, initial dye concentration, contact time, temperature, ion selectivity, and ionic strength and cation on adsorption process have been investigated during the batch adsorption study. Dye concentration of the filtrate was analyzed using a spectrophotometer ($\lambda_{\max, CV}$ 590 nm and $\lambda_{\max, SF}$ 517 nm). The uptake amount of dye per unit of adsorbent (q_e ; mg/g) was calculated by the following equation:

$$q_e = \frac{(C_o - C_e) * V}{m} \quad (1)$$

where m is the mass of nZVI and magnetic yeast in g, V is the volume of dye solutions in L, C_o and C_e are the initial and equilibrium dye concentrations in mg/L, respectively.

2.4. Continuous studies

The continuous adsorption experiments were carried out using Plexiglas materials (3 cm internal diameter and 46 cm height) in column. The column was packed with equivalent to 10 g of nZVI-alginate and magnetic yeast-alginate hydrogel beads (8 cm bed height). The flow rate and initial dye concentration were kept constant at 2 mL/min and 50 mg/L, respectively. After saturation of the column, the nZVI-alginate and magnetic yeast-alginate hydrogel beads were regenerated using 0.1 M ethylenediaminetetraacetic acid (EDTA) at a flow rate of 2 mL/min. After regeneration, the bed was studied for a second cycle and the adsorption-regeneration study was repeated.

2.5. Adsorption isotherms

The Langmuir [Eq. (2)], Freundlich [Eq. (3)], and D-R [Eq. (4)] isotherm models were given in below [4]:

Langmuir isotherm:

$$q_e = \frac{Q_o b C_e}{1 + b C_e} \quad (2)$$

where Q_o (mg/g) is the maximum adsorption capacity and b (L/mg) is the Langmuir constant, respectively.

Freundlich isotherm:

$$q_e = k_f C_e^{1/n} \quad (3)$$

where k_f (L/g) is the adsorption diffusion coefficient and represents the quantity of adsorbed dye on adsorbent surface per unit equilibrium concentration, the other Freundlich constant $1/n$ represents the adsorption intensity or surface heterogeneity.

D-R isotherm:

$$q_e = q_{D-R} e^{\beta \epsilon^2} \quad (4)$$

where q_{D-R} (mol/g) is the maximum adsorption capacity, β (mol²/J²) is the constant. ϵ (J/mol) is the Polanyi potential and calculated by the following equation:

$$\epsilon = RT \ln(1 + 1/C_e) \quad (5)$$

The mean free energy (E (kJ mol⁻¹)) was calculated by:

$$E = \frac{1}{\sqrt{2\beta}} \quad (6)$$

2.6. Kinetic modeling

Kinetic data were investigated with Lagergren pseudo first order, pseudo second order, and intraparticle diffusion model [2].

The Lagergren pseudo-first-order kinetic model was calculated by:

$$\log(q_e - q_i) = \log q_e - \frac{k_1}{2.303} t \quad (7)$$

The pseudo-second-order kinetic model was calculated by:

$$\frac{t}{q_t} = \frac{1}{k_2(q_e)^2} + \frac{1}{q_e}t \quad (8)$$

Intraparticle diffusion model was calculated by:

$$qt = k_3t^{0.5} + C \quad (9)$$

where q_t (mg/g) values are the amounts of adsorbed ions at considered contact times, k_1 (min^{-1}) is the rate constant for Lagergren pseudo-first order kinetic, k_2 ($\text{g}\cdot\text{mg}^{-1}\cdot\text{min}^{-1}$) is the rate constant for pseudo-second order kinetic, k_3 ($\text{mg}/\text{g}\cdot\text{min}^{0.5}$) is the rate constant for intraparticle diffusion model, and C is the intercept.

2.7. Thermodynamics parameters

The ΔH° , ΔS° , and ΔG° using the equilibrium constant (K_d) were calculated [26]:

$$\ln K_d = \frac{\Delta S^\circ}{R} - \frac{\Delta H^\circ}{RT} \quad (10)$$

$$\Delta G^\circ = \Delta H^\circ - T\Delta S^\circ \quad (11)$$

where T is the reaction temperature.

3. Results and discussion

3.1. Characterization of nZVI and magnetic yeast

FTIR spectrums of the nZVI and magnetic yeast are presented in Fig. 1. The broad bands in the $3600\text{--}3200\text{ cm}^{-1}$ region and 1645 cm^{-1} are O-H group vibrations [27]. For the nZVI and CV-magnetic yeast, the peak at 2900 cm^{-1} is related to $-\text{CH}_2-$ stretching. The 2100 cm^{-1} bands can be associated with stretching of alkynes ($\text{C}\equiv\text{C}$) or nitriles ($\text{C}\equiv\text{N}$). C-O stretching was observed in the $1300\text{--}1000\text{ cm}^{-1}$ region. For the magnetic yeast, the bands at around 1900 cm^{-1} and 1630 cm^{-1} were assigned to C-C and $-\text{C}=\text{O}$, C-N (amide I) stretching, respectively. The weaker bands at $<900\text{ cm}^{-1}$ are reduced Fe hydroxide formation [27]. These peaks in the FTIR spectrum demonstrated cooperation between *S. cerevisiae* and iron particles.

The SEM images of the nZVI and magnetic yeast are shown in Fig. 2. The nZVI composites were aggregated from van der Waals and magnetic forces [13]. SEM images of the magnetic yeast revealed the spherical shapes of *S. cerevisiae*. These shapes were connected in chains of beads, which were the result of the magnetic and van der Waals interactions between nZVI and *S. cerevisiae*. In addition, the magnetic yeast has quite rough and smooth surfaces.

The BET, total pore volume, and average pore diameter for the nZVI were $14.98\text{ m}^2/\text{g}$, $0.1399\text{ cm}^3/\text{g}$, and 37 nm ; for the magnetic yeast they were $21.01\text{ m}^2/\text{g}$, $0.0411\text{ cm}^3/\text{g}$, and 8 nm , respectively. The BET of magnetic yeast was 1.4 times higher than that of nZVI. At the same time, total pore volume and average pore diameter were lower for the magnetic yeast.

The EDX analysis for nZVI and the magnetic yeast indicated the presence of Fe, O, Na, C, and Cl (Fig. 3). The differences in peaks confirm the binding of CV and SF to the surface of nZVI and the magnetic yeast.

3.2. Batch studies

3.2.1. Effects of pH and contact time

The effects of initial pH (4, 6, and 8) were examined with contact times of 5, 15, 30, 60, 120, and 180 min. The impact of these two variables on adsorption is presented in Fig. 4.

After 180 min at pH 4, 6 and 8, the nZVI removed 58, 64, and 65% of CV and 77, 72, and 74% of SF; the magnetic yeast removed 99, 98, and 98% of CV and 90, 93, and 92% of SF, respectively. Hence there was no significant change in removal efficiency with greater pH. The nZVI removal efficiency was greater for SF than CV, and the opposite for the magnetic yeast. This is due to the relationship between the dye molecules and the surface of adsorbent. At these pH levels, the removal efficiency of nZVI was low. The removal efficiency can clearly be improved by combining nZVI with *S. cerevisiae*. The result is of great significance for removing CV and SF over a wide pH range. The points of zero charges (pH_{PZC}) of the nZVI and magnetic yeast were 9.47 and 9.40, respectively. At pH higher than pH_{PZC} , the adsorbent surface charge is negative while at lower pH values the charge is positive [28]. CV and SF are cationic dyes and have a pKa of 0.8 and 5.28, respectively [11]. At pH 0–2, CV is in the form of $\text{CV}^{3+}\cdot 3\text{Cl}^-$; for pH 2–9, CV is in the form of $\text{CV}^{2+}\cdot 2\text{Cl}^-$ and $\text{CV}^+\cdot\text{Cl}^-$; at pH > 9, CV is in the form of $\text{CV}\cdot\text{OH}$ [29]. Thus, the probable form of CV in the aqueous solutions is $\text{CV}^{2+}\cdot 2\text{Cl}^-$ and $\text{CV}^+\cdot\text{Cl}^-$. In this case, the adsorption mechanism occurs partly by ion exchange by releasing exchangeable protons and partly via surface complexation [30]. These results indicate that pH values were not a limiting factor in high efficiency dye removal; therefore strict pH control is unnecessary. This is an important advantage for practical applications [28]. For these reasons, only the most efficient pH values were used for subsequent experiments: pH 6 for CV removal by nZVI and magnetic yeast, pH 4 for SF removal by nZVI, and pH 6 for magnetic yeast. The removal efficiency and adsorption capacities for CV and SF dyes of magnetic yeast increased with contact time. The adsorption rate is related to the availability of active sites on the adsorbent surface [28].

3.2.2. Effect of amount

The effect of adsorbent amount was studied by varying the amount of nZVI and magnetic yeast from 1.0 to 15 g/L at a fixed initial concentration of 50 mg/L. The results are given in Fig. 5. Generally, increasing the adsorbent amount resulted in higher adsorption efficiency. This is because there are more sites available for dye adsorption [31]. At lower adsorbent amount, most of the active sites of adsorbent are utilized. At higher adsorbent amount, the active sites are much more than the saturated threshold adsorption point, and available dye molecules were insufficient to cover all the active sites. Both of the reasons result in the increase in removal efficiencies [32]. For CV, the optimum amounts of were 10 g/L of both nZVI and magnetic yeast;

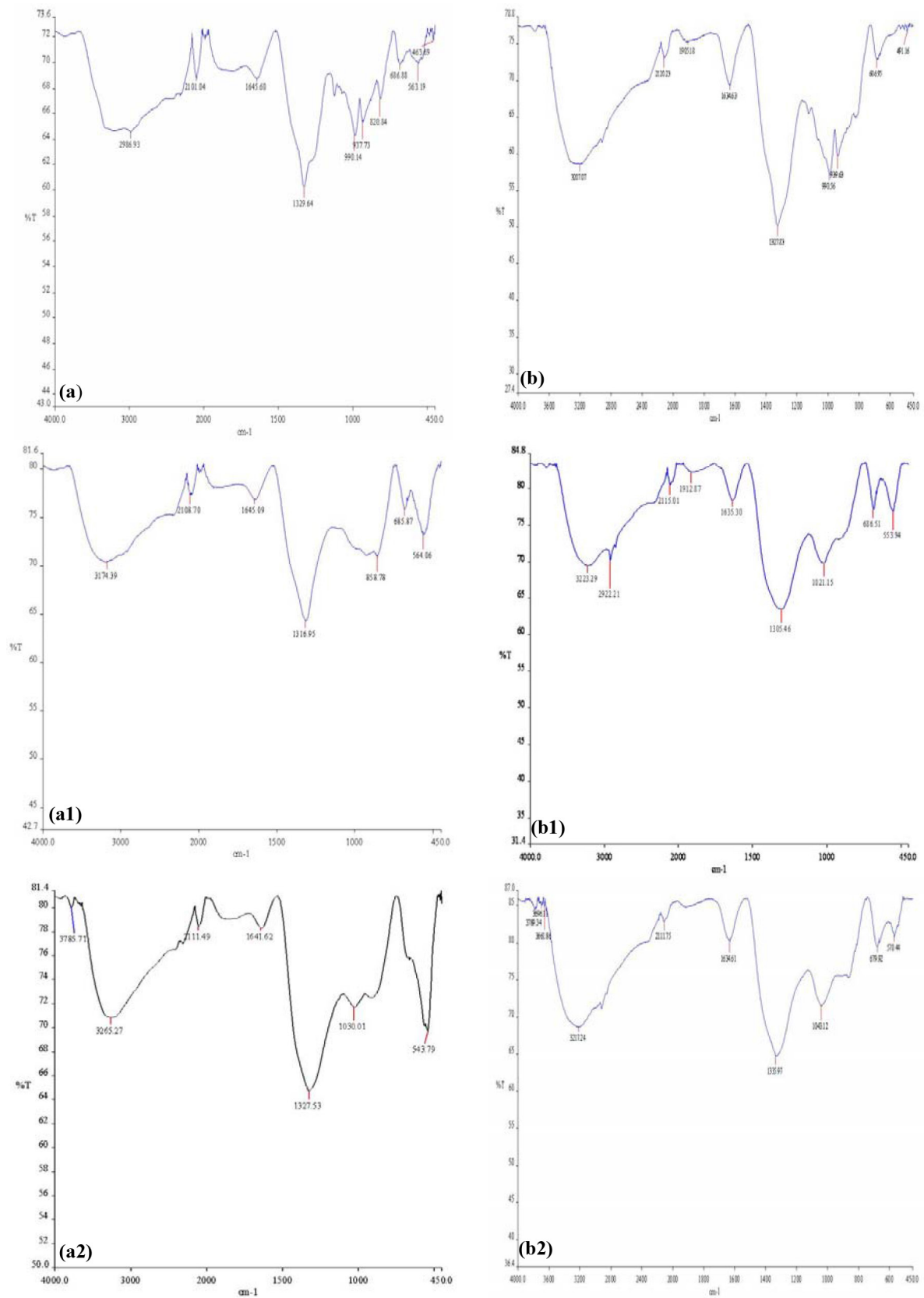


Fig. 1. Comparison of FTIR spectra of nZVI (a), CV-nZVI (a1), SF-nZVI (a2), magnetic yeast (b), CV-magnetic yeast (b1), SF-magnetic yeast (b2).

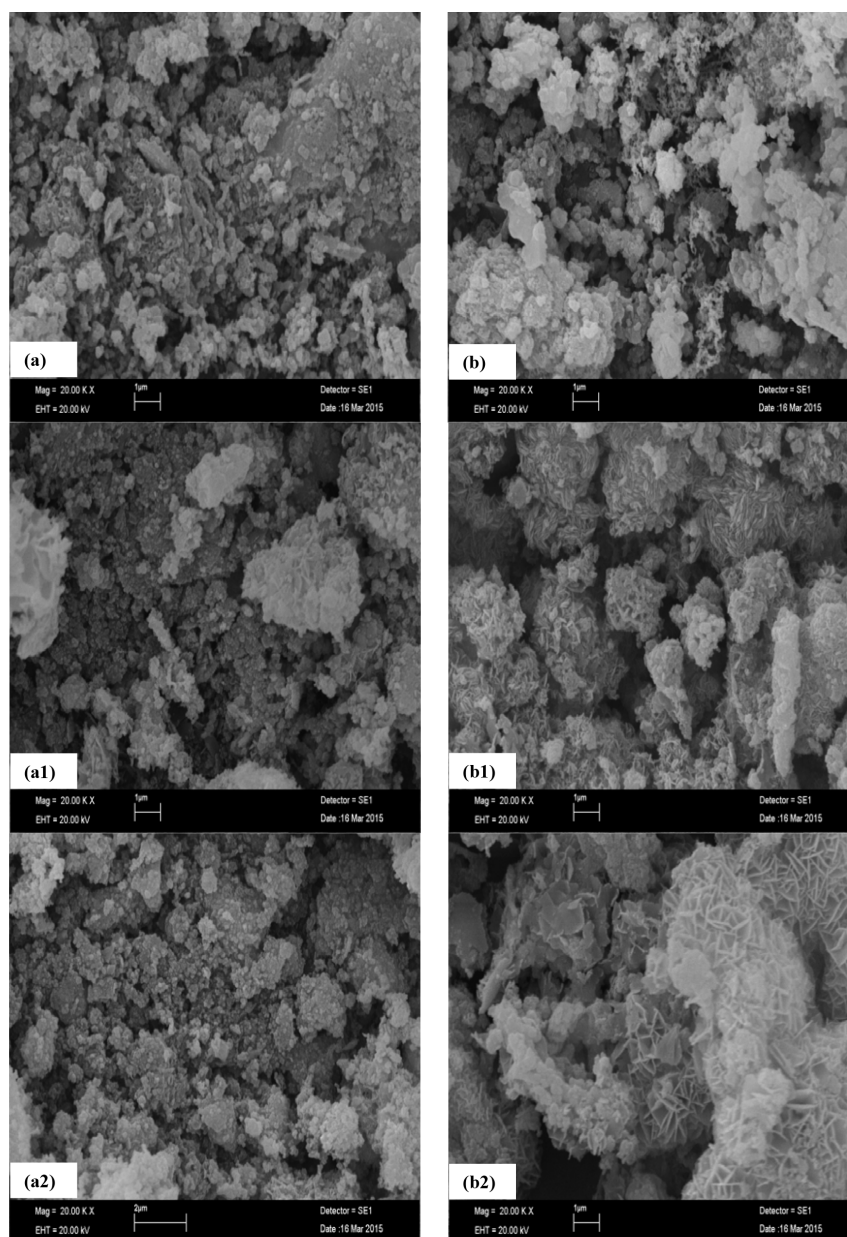


Fig. 2. Micrographs obtained by SEM of nZVI (a), CV-nZVI (a1), SF- nZVI (a2), magnetic yeast (b), CV-magnetic yeast (b1), SF-magnetic yeast (b2).

for SF, they were 10 g/L of nZVI and 5 g/L of magnetic yeast.

3.2.3. Effects of initial dye concentration

The effect of initial dye concentration on adsorption efficiency was examined for concentrations of 5–300 mg/L at 25°C (Fig. 5). Removal efficiency decreases as initial dye concentration increases. At lower dye concentrations, available surface area is high. At higher dye concentrations, available adsorbent sites are fewer so removal efficiency depends on initial dye concentration [31].

3.2.4. Effects of salt and cation concentration

Generally, wastewaters with dyes have high salt and metal concentrations. For this reason, the effect of salt and cation concentration was studied by adding 0.1–1 M NaCl and Cu^{2+} to the initial solutions (Fig. 6).

The effects of NaCl and Cu^{2+} ions on adsorption were very similar. They enhanced the CV and SF uptake by nZVI and magnetic yeast at pH 4. As a transitional metal cation, Cu^{2+} could have played a bridging role [33]. Cl^- could not have played a bridging role like Cu^{2+} but probably filled more adsorption points, thus increasing the adsorption of CV and SF dye onto the adsorbent [33].

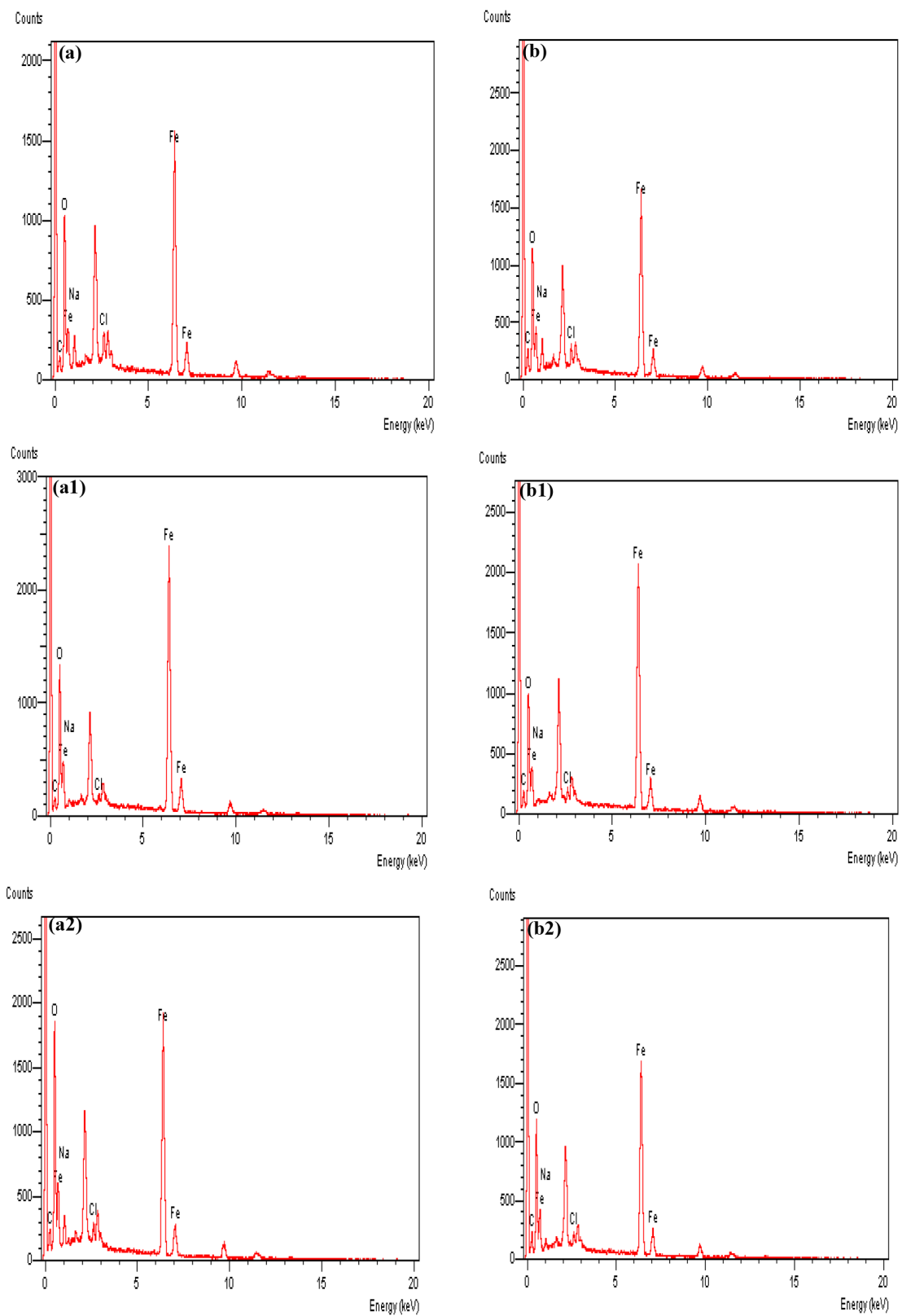


Fig. 3. EDX patterns of nZVI (a), CV-nZVI (a1), SF- nZVI (a2), magnetic yeast (b), CV-magnetic yeast (b1), SF-magnetic yeast (b2).

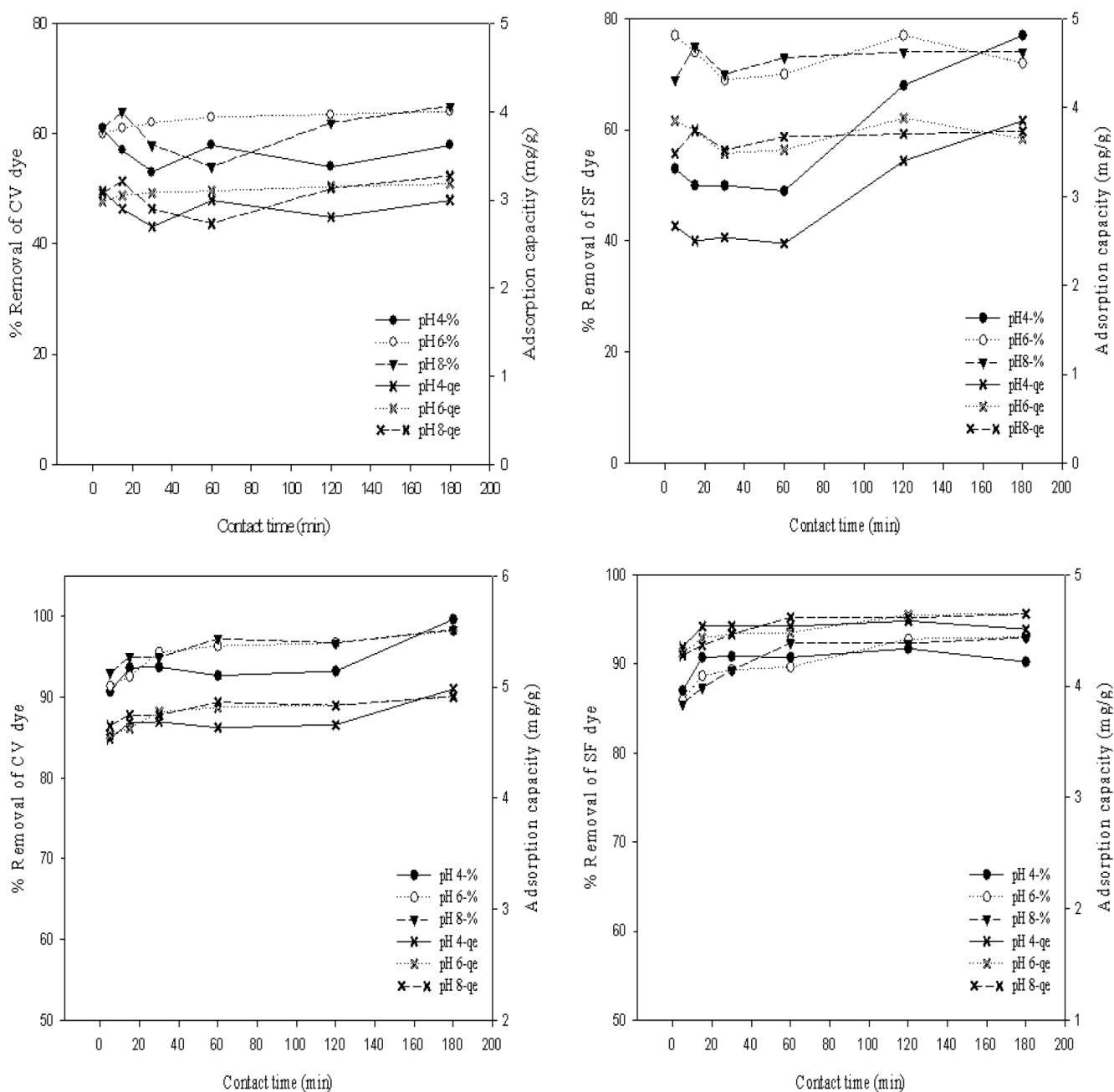


Fig. 4. Effect of initial pH and contact time on adsorption of CV and SF dye by nZVI and magnetic yeast, respectively (Experimental conditions: $C_0 = 50$ mg/L, $m = 10$ g/L, 298 K).

3.3. Isotherm study

The isotherm modeling parameters and plots are presented in Table 1 and Fig. 7a–d. Table 1 shows that the equilibrium data fit well to both Langmuir and Freundlich adsorption models (all $R^2 > 0.949$). Thus, adsorption occurred under homogeneous and monolayer surfaces. The effect of physical and chemical adsorption is combined [18,34]. The Q_m values of nZVI and magnetic yeast for CV and SF were 98, 122, 124, and 265 mg/g, respectively. SF had a higher maximum adsorption capacity than CV because of its chemical

structure and adsorbent affinity. The value of n is related to the distribution of bonded ions on the adsorbent surface. In general, $n < 1$ suggests that adsorption is favorable; the lower the n , the stronger the adsorption intensity [35]. According to D–R isotherm constants for $E < 8$ kJ/mol, physisorption controls the adsorption mechanism, but when E is between 8–16 kJ/mol, chemisorptions processes are involved [36]. The E values for nZVI and magnetic yeast were 7.97, 7.93, 8.90, and 8.46 kJ/mol for CV and SF dyes, respectively. Table 2 summarizes the maximum adsorption capacities for the various materials. It is evident nZVI and magnetic yeast has higher adsorption capacities than many other adsorbents.

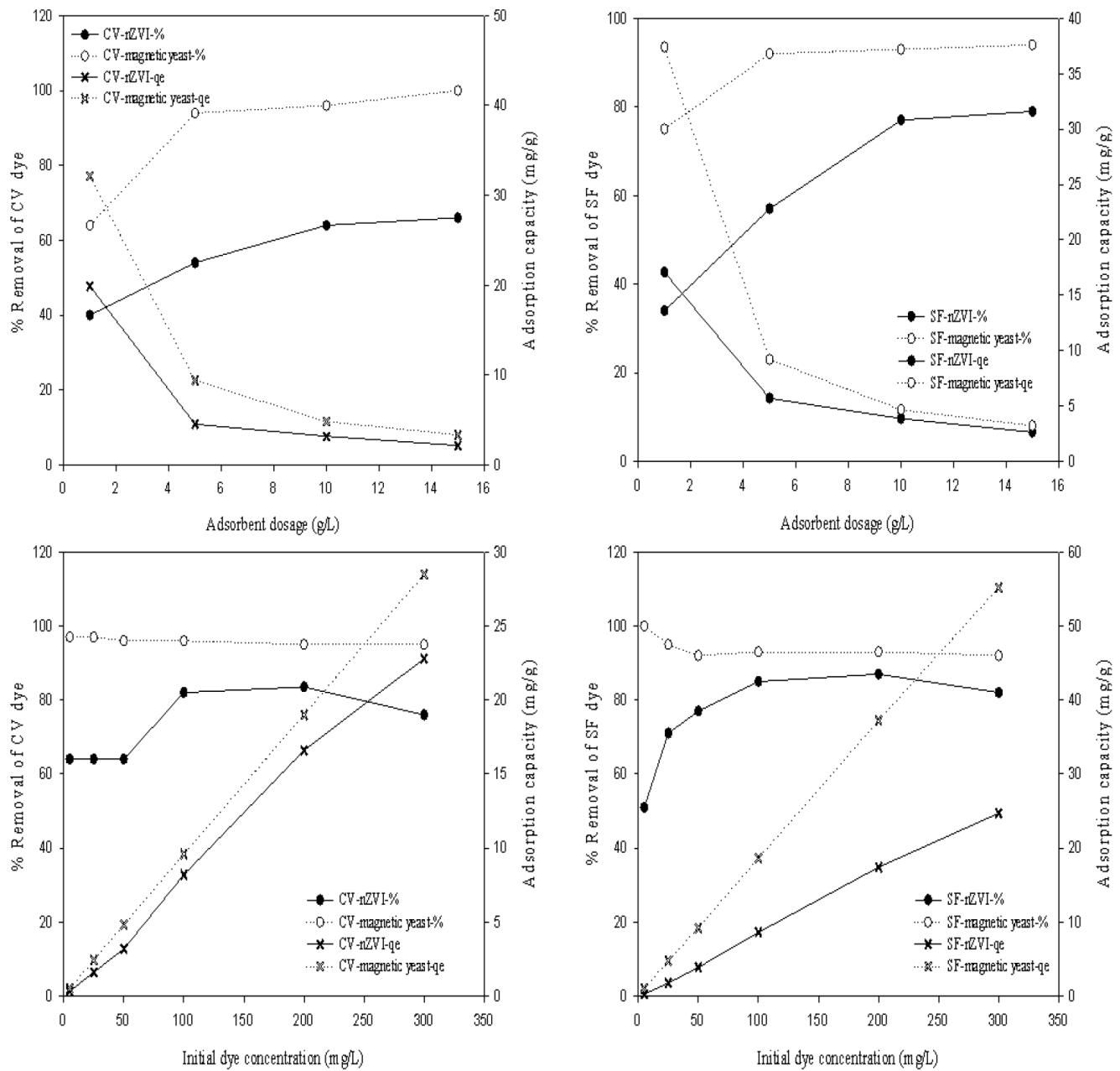


Fig. 5. Effect of adsorbent amount and initial dye on adsorption of CV and SF dye by nZVI and magnetic yeast.

3.4. Adsorption kinetics

The kinetic constants and R^2 values are given in Table 3, which show that the adsorption processes can be described as pseudo-second-order equations. The theoretical q_e values show good agreement with the experimental q_e values, confirming that adsorption follows the pseudo-second-order kinetic model. This indicates that the rate-determining step was surface adsorption [2]. According to Eq. (9), if a plot of q_t versus $t^{0.5}$ shows a straight line ($C = 0$) that passes through the origin, the adsorption mechanism is intraparticle diffusion. If not ($C \neq 0$), it means that there are intraparticle diffusion and boundary layer effects. As the

intercept value (C) increases, the effect of surface sorption in the rate-controlling step increases (Fig. 7e) [2,43,44]. In this study, intraparticle diffusion was involved, but it was not the sole rate-controlling step. Both intraparticle diffusion and boundary diffusion models are involved.

3.5. Thermodynamic studies

In terms of thermodynamic parameters, the positive value of ΔH° indicates that adsorption was endothermic (Table 4). The positive entropy (ΔS°) show that randomness increased (adsorbat/adsorbent) during adsorption. Nega-

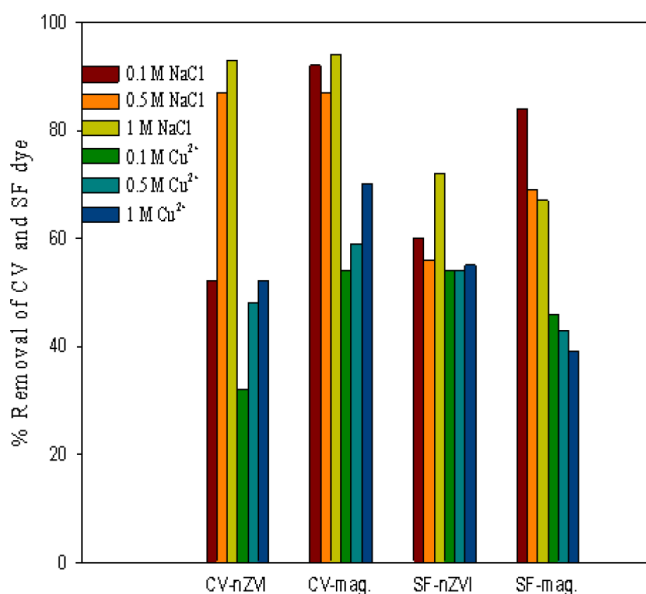


Fig. 6. Effect of salt (NaCl) and cation (Cu²⁺) concentration.

Table 1
Langmuir, Freundlich and D-R isotherm model parameters for nZVI and magnetic yeast

Model	nZVI		Magnetic yeast	
	CV	SF	CV	SF
Langmuir				
Q_m (mg/g)	98	122	124	265
b (L/mg)	0.004	0.005	0.002	0.011
R^2	0.953	0.969	0.998	0.998
Freundlich				
k_f (L/g)	0.503	0.643	2.801	3.383
$1/n$	0.90	0.93	0.85	0.88
R^2	0.949	0.966	0.999	0.997
D-R				
q_{D-R} (mol/g)	0.002	0.003	0.004	0.008
E (kJ/mol)	7.97	7.93	8.90	8.46
β (mol ² /J ²)	7.8688 $\times 10^{-9}$	7.9602 $\times 10^{-9}$	6.3085 $\times 10^{-9}$	6.9878 $\times 10^{-9}$
R^2	0.953	0.971	0.998	0.998

tive values of ΔG° indicate that adsorption was thermodynamically spontaneous and feasible [45].

3.6. Continuous column studies

3.6.1. Breakthrough curve modeling

A successful adsorption process requires predicting the breakthrough curve for the effluent [45,46]. Continu-

Table 2
Comparison of maximum adsorption capacities (Q_o) of nZVI and magnetic yeast with other adsorbents

Adsorbent	Q_o (mg/g)	References
CV		
nZVI	98	Present study
Magnetic yeast	124	Present study
Jackfruit leaf powder	43.40	[2]
Multifunctional kaolinite-supported nanoscale zero-valent iron	129	[18]
Magnetic calcium ferrite nanoparticle	0.83	[28]
NaOH modified rice husk	41.5	[37]
ZVI-GAM	172.4	[38]
Bentonite-alginate	630	[39]
Peanut hull waste biomass	100	[40]
SF		
nZVI	122	Present study
Magnetic yeast	265	Present study
Calcined bones	93	[1]
Kaolinite clay	16	[11]
Calcined mussel shells	154	[31]
Graphene oxide-chitosan	279	[41]
Ni:FeO(OH)-NWs	35	[42]

ous system for modeling studies were performed at the flow rate of 2 mL/min with an influent concentration of 50 mg/L and a bed depth of 8 cm (equal to 10 g nZVI-alginate and magnetic yeast-alginate hydrogel beads) at room temperature (25°C) (Fig. 8). The time to reach C_t/C_o was significantly higher for SF than CV. The column adsorption capacity (q_e ; mg/g) for CV and SF of nZVI-alginate and magnetic yeast-alginate was calculated from the column experiments [Eq. (15)]

$$q_e = \frac{Q[(t \times C_o) - C_{total}]}{m} \quad (12)$$

where C_o and C_{total} are the initial and effluent concentrations (mg/L), respectively; t is the time (h), Q is the flow rate (L/h).

Column adsorption capacities ($q_{e,c}$) for CV and SF of nZVI-alginate and magnetic biosorbent-alginate were 8.88, 10.11, 19.28, and 15.31 mg/g, respectively. As shown, the adsorption capacities of magnetic yeast-alginate were higher than the adsorption capacities of nZVI-alginate. This can be explained through synergy between nZVI and *S. cerevisiae* yeast. This shows that these materials are quite successful in removing dye from wastewater.

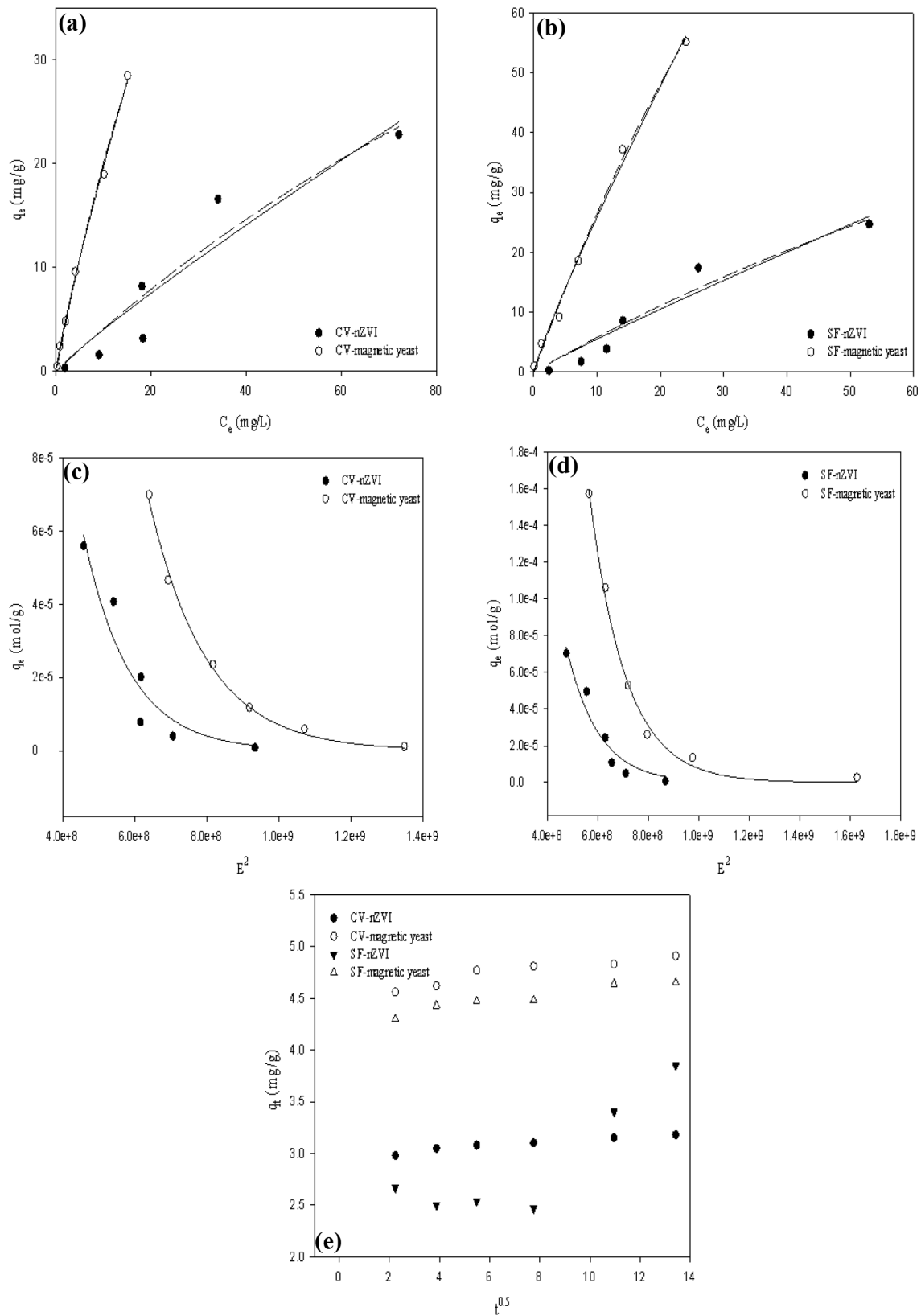


Fig. 7. Isotherm (a,b,c,d) and intraparticle diffusion model (e) plots for adsorption of CV and SF onto nZVI and magnetic yeast.

Table 3
Pseudo-first model, pseudo-second model and intra particle diffusion model parameters

Model	nZVI		Magnetic yeast	
	CV	SF	CV	SF
$q_{e,exp}$ (mg/g)	3.18	3.85	4.81	4.65
Pseudo-first order				
k_1 (min ⁻¹)	0.014	0.007	0.012	0.027
$q_{e,cal}$ (mg/g)	0.18	1.50	0.29	0.45
R^2	0.965	0.714	0.779	0.900
Pseudo-second order				
k_2 (g·mg ⁻¹ ·min ⁻¹)	0.340	0.017	0.210	0.183
$q_{e,cal}$ (mg/g)	3.19	3.96	4.92	4.67
R^2	0.999	0.968	0.999	0.999
Intra particle diffusion				
k_i (mg/g·min ^{0.5})	0.016	0.116	0.029	0.029
C	2.972	2.060	4.533	4.277
R^2	0.941	0.735	0.869	0.919

Table 4
Thermodynamic parameters obtained for CV and SF adsorption onto nZVI and magnetic yeast

	nZVI		Magnetic yeast	
	CV	SF	CV	SF
ΔH° (kJ/mol)	62.27	-21.08	106.92	24.78
ΔS° (kJ/mol.K)	0.251	0.022	0.427	0.142
ΔG° (kJ/mol)				
298 K	-12.51	-14.09	-18.99	-17.44
308 K	-15.09	-15.09	-27.10	-19.27
318 K	-17.62	-13.56	-27.74	-20.34

3.7. Regeneration of the nZVI-alginate and magnetic yeast-alginate

The regeneration and reuse of materials is important in adsorption [47]. The regeneration and reusability of the yeast were studied. The nZVI-alginate and magnetic yeast-alginate were tested in two cycles using 0.1 M EDTA solution at a flow rate of 2 mL/min. Regeneration efficiency was calculated for both cycles (Table 5) and determined with Eq. (16) [47]:

$$RE(\%) = \frac{q_{reg}}{q_{org}} \times 100 \quad (13)$$

where q_{reg} is the adsorptive capacity of the regenerated column and q_{org} is the original capacity (mg/g) of the adsorbent.

After two cycles, regeneration efficiency was 76–87% and breakthrough time, breakthrough uptake capacity, and exhaustion time decreased. Decline of breakthrough time shows decreased adsorption performance. This may be due to the dissolution of some soluble constituents such as iron oxide, *S. cerevisiae* and alginate in nZVI, and magnetic yeast during regeneration [48].

3.8. Mechanisms of adsorption

The role of nZVI particles in the dye adsorption mechanism is proposed as follows: (i) strong reductive with the oxidation of Fe⁰ to Fe³⁺, (ii) micro-electrolysis, and (iii) surface complexation via hydroxyl groups on the shell of nZVI and flocculation process [49]. nZVI particles with high surface activity can directly react with dye molecules. The reaction between Fe⁰ and H₂O or H⁺ ions can induce destroying the chromophore group. During the reaction formed iron oxides could also adsorb dye molecules via the sulfonic group [49]. In addition to the above, a further mechanism may be added for the dye removal process of the magnetic yeast: (iv) biosorption by functional groups on the yeast cells, (v) diffusion into the Fe⁰ core and yeast cell wall [20,24]. The reason for the higher adsorp-

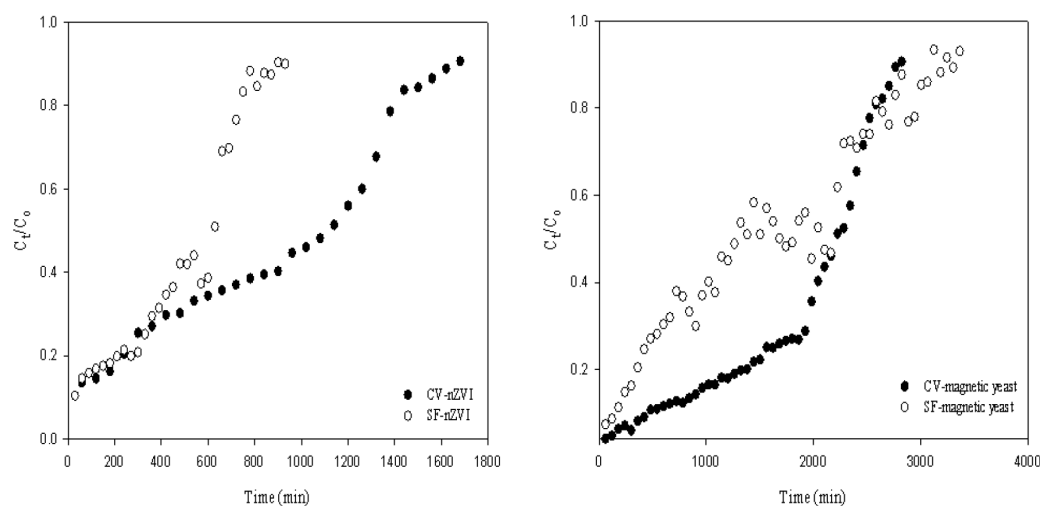


Fig. 8. Breakthrough curves for CV and SF adsorption onto nZVI-alginate and magnetic yeast-alginate.

Table 5
Regeneration-reusability parameters for two cycles

Cycle	Parameter	nZVI-alginate		Magnetic yeast-alginate	
		CV	SF	CV	SF
1	Breakthrough uptake (mg/g)	7.64	5.08	17.19	12.39
	Breakthrough time (min)	1140	660	2220	1320
	Bed exhaustion time (min)	1680	930	2820	3360
	q_{reg} (mg/g)	8.88	10.11	19.28	15.31
	Regeneration efficiency (%)	Original	Original	Original	Original
2	Breakthrough uptake (mg/g)	4.11	2.02	13.61	9.17
	Breakthrough time (min)	240	210	720	720
	Bed exhaustion time (min)	600	750	900	1380
	q_{reg} (mg/g)	6.84	8.18	14.69	13.33
	Regeneration efficiency (%)	77	81	76	87

Breakthrough time: 50% of initial concentration C_0 .

tion capacity of magnetic yeast was synergistic effect of between iron particles and functional groups of *S. cerevisiae* yeast.

4. Conclusion

In this study, nZVI and nZVI-modified *S. cerevisiae* composite nanoparticles with average diameters of 37 nm and 8 nm, respectively had successfully prepared and applied to remove organic dyes. The composites obtained were characterized using FT-IR, SEM and EDX. Initial solution pH, contact time, initial dye concentration, adsorbent amount and adsorption temperature played important roles on dyes adsorption onto the composites. The Q_0 values for CV and SF dyes at optimum conditions were 98, 122, 124, and 265 mg/g, respectively. The maximum adsorption capacities of nZVI and magnetic yeast were higher than many other materials under similar conditions. The kinetics study showed that the adsorption follows a pseudo-second order model better than a pseudo-first order model. The application of an intraparticle diffusion model further confirms that the rate-determining step of the adsorption was probably not mass transfer diffusion. Furthermore, the results indicate that there is chemisorption and electrostatic attraction in the dye adsorption process, and that the dye adsorption processes on nZVI and magnetic yeast are feasible and spontaneous. The positive entropy (ΔS°) suggests that randomness increased. The dye removal in the continuous mode was studied. The column adsorption capacities of magnetic yeast were higher than the adsorption capaci-

ties of nZVI because of the synergistic effects of functional groups from *S. cerevisiae* yeast. The adsorption-regeneration studies confirmed the reusability potential of the composites for the removal of CV and SF from aqueous solution. Therefore, nZVI and magnetic yeast composites are efficient and practical to be an economical and effective adsorbents for the rapidly removal of toxic dyes from the effluents of textile and other industries.

Acknowledgment

This study was supported by Cumhuriyet University, Scientific Research Project Funding (CUBAP/M-547).

References

- [1] M. El Haddad, R. Slimani, R. Mamouni, R. Laamari, S. Rafqah, S. Lazar, Evaluation of potential capability of calcined bones on the biosorption removal efficiency of safranin as cationic dye from aqueous solutions, *J. Taiwan Inst. Chem. Eng.*, 44 (2013) 13–18.
- [2] P. Das Saha, S. Chakraborty, S. Chowdhury, Batch and continuous (fixed-bed column) biosorption of crystal violet by *Artocarpus heterophyllus* (jackfruit) leaf powder, *Colloid. Surface. B., Biointerfaces*, 92 (2012) 262–270.
- [3] G.O. El-Sayed, Removal of methylene blue and crystal violet from aqueous solutions by palm kernel fiber, *Desalination*, 272 (2011) 225–232.
- [4] T.A. Khan, E.A. Khan, Shahjahan, Removal of basic dyes from aqueous solution by adsorption onto binary iron-manganese oxide coated kaolinite, non-linear isotherm and kinetics modeling, *Appl. Clay Sci.*, 107 (2015) 70–77.
- [5] S. Shariati, M. Faraji, Y. Yamini, A.A. Rajabi, Fe_3O_4 magnetic nanoparticles modified with sodium dodecyl sulfate for removal of safranin O dye from aqueous solutions, *Desalination*, 270 (2011) 160–165.
- [6] G. Sudarjanto, B. Keller-Lehmann, J. Keller, Optimization of integrated chemical-biological degradation of a reactive azo dye using response surface methodology, *J. Hazard. Mater. B*, 138 (2006) 160–168.
- [7] A. Szygula, E. Guibal, M.A. Palacin, M. Ruiz, A.M. Sastre, Removal of an anionic dye (Acid Blue 92) by coagulation-flocculation using chitosan, *J. Environ. Manage.*, 90 (2009) 2979–2986.
- [8] M. Karatas, Y.A. Argun, M.E. Argun, Decolorization of antraquinonic dye, Reactive Blue 114 from synthetic wastewater by Fenton process, kinetics and thermodynamics, *J. Ind. Eng. Chem.*, 18 (2012) 1058–1062.
- [9] A.H. Essadki, M. Bennajah, B. Gourich, C. Vial, M. Azzi, H. Delmas, Electrocoagulation/electroflotation in an external-loop airlift reactor-application to the decolorization of textile dye wastewater, A case study, *Chem. Eng. Process.*, 47 (2008) 1211–1223.
- [10] A. Wang, J. Qu, H. Liu, J. Ge, Degradation of azo dye acid red 14 in aqueous solution by electrokinetic and electrooxidation process, *Chemosphere*, 55 (2004) 1189–1196.
- [11] K.O. Adebawale, B.I. Olu-Owolabi, E.C. Chigbundu, Removal of safranin-O from aqueous solution by adsorption onto kaolinite clay, *J. Encapsul. Ads. Sci.*, 4 (2014) 89–104.
- [12] T. Liu, Z.L. Wang, X. Yan, B. Zhang, Removal of mercury (II) and chromium (VI) from wastewater using a new and effective composite, Pumice-supported nanoscale zero-valent iron, *Chem. Eng. J.*, 245 (2014) 34–40.
- [13] T. Wang, J. Sua, X. Jin, Z. Chen, M. Megharaj, R. Naidu, Functional clay supported bimetallic nZVI/Pd nanoparticles used for removal of methyl orange from aqueous solution, *J. Hazard. Mater.*, 262 (2013) 819–825.

- [14] E.J. Petersena, R.A. Pinto, X. Shi, Q. Huange, Impact of size and sorption on degradation of trichloroethylene and polychlorinated biphenyls by nano-scale zerovalent iron, *J. Hazard. Mater.*, 243 (2012) 73–79.
- [15] Z. Suna, S. Zheng, G.A. Ayokob, R.L. Frost, Y. Xi, Degradation of simazine from aqueous solutions by diatomite-supported nanosized zero-valent iron composite materials, *J. Hazard. Mater.*, 263 (2013) 768–777.
- [16] T. Liu, L. Zhao, D. Sun, X. Tan, Entrapment of nanoscale zero-valent iron in chitosan beads for hexavalent chromium removal from wastewater, *J. Hazard. Mater.*, 184 (2010) 724–730.
- [17] S.R. Kanel, D. Nepal, B. Manning, H. Choi, Transport of surface-modified nanoparticle in porous media and application to arsenic (III) remediation, *J. Nanopart. Res.*, 9 (2007) 725–735.
- [18] Z. Chen, T. Wang, X. Jin, Z. Chen, M. Megharaj, R. Naidu, Multifunctional kaolinite-supported nanoscale zero-valent iron used for the adsorption and degradation of crystal violet in aqueous solution, *J. Colloid. Interface. Sci.*, 398 (2013) 59–66.
- [19] Y. Li, J. Li, Y. Zhang, Mechanism insights into enhanced Cr(VI) removal using nanoscale zero-valent iron supported on the pillared bentonite by macroscopic and spectroscopic studies, *J. Hazard. Mater.*, 227–228 (2012) 211–218.
- [20] A. Rao, A. Bankar, A.R. Kumar, S. Gosavi, S. Zinjarde, Removal of hexavalent chromium ions by *Yarrowia lipolytica* cells modified with phyto-inspired Fe⁰/Fe₃O₄ nanoparticles, *J. Contam. Hydrol.*, 146 (2013) 63–73.
- [21] H. Yavuz, A. Denizli, H. Gungunes, M. Safarikova, I. Safarik, Biosorption of mercury on magnetically modified yeast cells, *Sep. Purif. Technol.*, 52 (2006) 253–260.
- [22] I. Safarik, L.F.T. Rego, M. Borovska, E. Mosiniewicz Szablewska, F. Weyda, M. Safarikova, New magnetically responsive yeast-based biosorbent for the efficient removal of water-soluble dyes, *Enzyme Microb. Technol.*, 1–40 (2007) 1551–1556.
- [23] Q. Peng, Y. Liu, G. Zeng, W. Xu, C. Yang, J. Zhang, Biosorption of copper (II) by immobilizing *saccharomyces cerevisiae* on the surface of chitosan-coated magnetic nanoparticles from aqueous solution, *J. Hazard. Mater.*, 177 (2010) 676–682.
- [24] U.A. Guler, M. Ersan, *S. cerevisiae* cells modified with nZVI, a novel magnetic biosorbent for nickel removal from aqueous solutions, *Desal. Water Treat.*, 57(16) (2016) 7196–7208
- [25] Ç. Üzüüm, T. Shahwan, A.E. Eroglu, K.R. Hallam, T.B. Scott, I. Lieberwirth, *S. cerevisiae* cells modified with nZVI, a novel magnetic biosorbent for nickel removal from aqueous solutions, *Desal. Water Treat.*, 1 (2009) 13–18.
- [26] L. Cottet, C.A.P. Almeida, N. Naidek, M.F. Viante, M.C. Lopes, N.A. Debacher, Adsorption characteristics of montmorillonite clay modified with iron oxide with respect to methylene blue in aqueous media, *Appl. Clay Sci.*, 95 (2014) 25–31.
- [27] S.A. Kim, S. Kamala Kannan, K.J. Lee, Y.J. Park, P.J. Shea, W.H. Lee, H.M. Kim, B.T. Oh, Removal of Pb (II) from aqueous solution by a zeolite–nanoscale zero-valent iron composite, *Chem. Eng. J.*, 217 (2013) 54–60.
- [28] S. An, X. Liu, L. Yang, L. Zhang, Enhancement removal of crystal violet dye using magnetic calcium ferrite nanoparticle, Study in single and binary solute systems, *Chem. Eng. Res. Des.*, 94 (2015) 726–735.
- [29] B.C.S. Ferreira, F.S. Teodoro, A.B. Mageste, L.F. Gil, R.P.L. De Freitas, V.A. Gurgel, Application of a new carboxylate-functionalized sugarcane bagasse for adsorptive removal of crystal violet from aqueous solution, kinetic, equilibrium and thermodynamic studies, *Ind. Crop. Prod.*, 65 (2015) 521–534.
- [30] M. Ghaedi, S. Hajati, B. Barazesh, F. Karimi, G. Ghezlbash, *Saccharomyces cerevisiae* for the biosorption of basic dyes from binary component systems and the high order derivative spectrophotometric method for simultaneous analysis of Brilliant green and Methylene blue, *J. Ind. Eng. Chem.*, 19 (2013) 227–233.
- [31] M. El Haddad, A. Regti, R. Slimani, S. Lazar, Assessment of the biosorption kinetic and thermodynamic for the removal of safranin dye from aqueous solutions using calcined mussel shells, *J. Ind. Eng. Chem.*, 20 (2014) 717–724.
- [32] J. Zhou, Q.F. Lü, J.J. Luo, Efficient removal of organic dyes from aqueous solution by rapid adsorption onto polypyrrole-based composites, *J. Clean. Prod.*, 167 (2017) 739–748.
- [33] X. Song, D. Liu, G. Zhang, M. Frigon, X. Meng, K. Li, Adsorption mechanisms and the effect of oxytetracycline on activated sludge, *Bioresource Technol.*, 151 (2014) 428–431.
- [34] A.S. Ozcan, O. Gok, A. Ozcan, Adsorption of lead (II) ions onto 8-hydroxy quinoline immobilized bentonite, *J. Hazard. Mater.*, 161 (2009) 499–509.
- [35] W.T. Tsai, C.W. Lai, K.J. Hsien, Effect of particle size of activated clay on the adsorption of paraquat from aqueous solution, *J. Colloid Interface Sci.*, 263 (2003) 29–34.
- [36] A. Mittal, D. Kaur, A. Malviya, J. Mittal, V.K. Gupta, Adsorption studies on the removal of coloring agent phenol red from wastewater using waste materials as adsorbents, *J. Colloid Interface Sci.*, 337 (2009) 345–354.
- [37] S. Chakraborty, S. Chowdhury, P. Das Saha, Adsorption of crystal violet from aqueous solution onto NaOH-modified rice husk, *Carbohydr. Polym.*, 86 (2011) 1533–1541.
- [38] J. Liu, Y. Wang, Y. Fang, T. Mwamulima, S. Song, C. Peng, Removal of crystal violet and methylene blue from aqueous solutions using the fly ash-based adsorbent material-supported zero-valent iron, *J. Mol. Liq.*, 250 (2018) 468–476.
- [39] R. Fabryanty, C. Valencia, F.E. Soetaredjo, J.N. Putro, S. Permatasari Santoso, A. Kurniawan, Y.H. Ju, S. Ismadji, Removal of crystal violet dye by adsorption using bentonite-alginate composite, *J. Env. Chem. Eng.*, 5 (2017) 5677–5687.
- [40] N. Tahir, H.N. Bhatti, M. Iqbal, S. Noreen, Biopolymers composites with peanut hull waste biomass and application for crystal violet adsorption, *Int. J. Biol. Macromol.*, 94 (2017) 210–220.
- [41] S. Debnath, K. Parashar, P. Kriveshini, Ultrasound assisted adsorptive removal of hazardous dye Safranin O from aqueous solution using crosslinked graphene oxide-chitosan (GO-CH) composite and optimization by response surface methodology (RSM) approach, *Carbohydr. Polym.*, 175 (2017) 509–517.
- [42] M. Dastkhoona, M. Ghaedi, A. Asfarama, M.H.A. Azqhandi, M. Kumar Purkait, Simultaneous removal of dyes onto nanowires adsorbent use of ultrasound assisted adsorption to clean waste water: Chemometrics for modeling and optimization, multicomponent adsorption and kinetic study, *Chem. Eng. Res. Des.*, 124 (2017) 222–237.
- [43] U.A. Guler, M. Sarioglu, Removal of tetracycline from wastewater using pumice stone, equilibrium, kinetic and thermodynamic studies, *J. Environ. Health*, 12 (2014) 79–83.
- [44] A. Murugesan, L. Ravikumar, V.S.S. Bala, P.S. Kumar, T. Vidhyadevi, S. Dinesh, S. Kirupha, S.S. Kalaivani, S. Krithiga, S. Sivanesan, Removal of Pb (II), Cu (II) and Cd (II) ions from aqueous solution using polyazomethine amides, Equilibrium and kinetic approach, *Desalination*, 271 (2011) 199–208.
- [45] E.D. Woumfo, J.M. Siewe, D. Njopwouo, A fixed-bed column for phosphate removal from aqueous solutions using an andosol-bagasse mixture, *J. Environ. Manage.*, 151 (2015) 450–460.
- [46] R. Han, L. Zou, X. Zhao, Y. Xu, F. Xu, Y. Li, Y. Wang, Characterization and properties of iron oxide-coated zeolite as adsorbent for removal of copper (II) from solution in fixed bed column, *Chem. Eng. J.*, 149 (2009) 123–131.
- [47] B. Kiran, A. Kaushik, Cyanobacterial biosorption of Cr (VI), Application of two parameter and Bohart Adams models for batch and column studies, *Chem. Eng. J.*, 144 (2008) 391–399.
- [48] T.C. Nguyen, P. Loganathan, T.V. Nguyen, S. Vigneswaran, J. Kandasamy, R. Naidu, Simultaneous adsorption of Cd, Cr, Cu, Pb, and Zn by an iron-coated Australian zeolite in batch and fixed-bed column studies, *Chem. Eng. J.*, 270 (2015) 393–404.
- [49] J. Fan, Y. Guo, J. Wang, M. Fan, Rapid decolorization of azo dye methyl orange in aqueous solution by nanoscale zerovalent iron particles, *J. Hazard. Mater.*, 166 (2009) 904–910.